Electronic Supplementary Information (ESI)

Dehydration-triggered magnetic phase conversion in the porous Cu(II)Mn(III) metal-organic framework

Dae Won Ryu,[a] Jin Ho Shin,[a] Kwang Soo Lim,[a] Woo Ram Lee,[a] Won Ju Phang,[a] Sung Won Yoon,[b] Byoung Jin Suh,[b] Eui Kwan Koh,[c] and Chang Seop Hong*,[a]

[a]Department of Chemistry, Korea University, Seoul 136-713, Korea; E-mail: cshong@korea.ac.kr
[b]Department of Physics, The Catholic University of Korea, Buchon 420-743, Korea
[c]Nano-Bio System Research Team, Korea Basic Science Institute, Seoul 136-713, Korea

$[Cu(Tt)_2][Mn(salen)]_2(ClO_4)_2 \cdot 7H_2O$ [**1**; Tt = tris(triazolyl)borate, salen = N,N'-ethylenebis(salicylideneiminato) dianion]: $[Mn(salen)(H_2O)](ClO_4)$ (36 mg, 0.08 mmol) dissolved in MeCN (10 mL) was mixed with $[Cu(Tt)_2]$ (20 mg, 0.04 mmol) in H_2O (10 mL). After stirring for 30 min, the solution was filtered and slowly evaporated at room temperature for 1 week. The dark brown crystals were obtained after filtration. Yield: 40%. Elemental analysis (%) calcd for $C_{44}H_{56}B_2Cl_2CuMn_2N_{22}O_{19}$: C 36.12, H 3.86, N 21.06; found: C 35.73, H 3.8, N 20.81.

$[Cu(Tt)_2][Mn(salen)]_2(ClO_4)_2$ (dehydrated phase; **1'**): **1** was heated at 90 °C under vacuum for 1 h. Elem ental analysis (%) calcd for $C_{44}H_{42}B_2Cl_2CuMn_2N_{22}O_{12}$: C 39.53, H 3.17, N 23.05; found: C 39.51, H 3.34, N 23.10. The resolvated phase was obtained by soaking **1'** in H_2O for 7 days.

Physical Measurements. Elemental analyses for C, H and N were performed at the Elemental Analysis Service Center of Sogang University. Infrared spectra were obtained from Nujol mull with a Bomen MB-104 spectrometer. Thermogravimetric analyses were carried out at a ramp rate of 10 °C/min in a N_2 flow using a Scinco TGA N-1000 instrument. PXRD data were recorded using Cu Kα (λ = 1.5406 Å) on a Rig aku Ultima III diffractometer with a scan speed of 2°/min and a step size of 0.02°. Magnetic susceptibilitie s for **1** and **1'** were carried out using a Quantum Design SQUID susceptometer (dc) and a PPMS magneto meter (ac). Diamagnetic corrections of all samples were estimated from Pascal's Tables.

Gas Sorption Measurements. Gas sorption isotherms were measured using a BEL Belsorp mini II gas adsorption instrument up to 1 atm of gas pressure. The highly pure N_2 (99.999%), H_2 (99.999%), CO_2 (99.9 99%), and CH_4 (99.995%) were used in the sorption experiments. N_2 and H_2 gas isotherms were measure d at 77 K and CO_2 was measured at 195 K. For N_2 and CO_2 the additional uptake isotherm and CH_4 uptak e isotherm was obtained at 273 K.

Crystallographic Structure Determination. To determine single crystal structure for **1'**, the sample w as prepared as follows. The single crystal of **1** was put in the capillary with one side open and the other si de of the entrance blocked. Then, the capillary was put in a vial. The vial was capped with septum and co nnected to a vacuum line to evacuate the crystal. The vial was placed in an oil bath and heated at 100 °C f or 3 hours. After the treatment, the capillary was sealed with a wax in a glove box. X-ray data for **1** and **1'** were collected on a Bruker SMART APEXII diffractometer equipped with graphite monochromated Mo Kα (λ = 0.71073 Å). Preliminary orientation matrix and cell parameters were determined from three sets o f ω scans at different starting angles. Data frames were obtained at scan intervals of 0.5° with an exposure time of 10 s per frame. The reflection data were corrected for Lorentz and polarization factors. Absorptio n corrections were carried out using SADABS. The structures of **1** and **1'** were solved by direct methods a nd refined by full-matrix least-squares analysis using anisotropic thermal parameters for non-hydrogen at oms with the SHELXTL program. All hydrogen atoms were calculated at idealized positions and refined with the riding models. Crystal data of **1**: Mr = 1490.07, T = 296 K, tetragonal, space group $I4_1/a$, a = 36. 102(6) Å, c = 9.930(3) Å, V = 12943(5) Å^3, Z = 8, D_{calc} = 1.529 g cm^{-3}, μ = 0.880 mm^{-1}, 25740 reflections collected, 7662 unique (R_{int} = 0.1116), $R1$ = 0.0716, $wR2$ = 0.1849 [$I > 2\sigma(I)$]. **1'**: Mr = 1336.94, T = 296 K, tetragonal, space group $I4_1/a$, a = 35.9978(6) Å, c = 9.9081(3) Å, V = 12839.3(5) Å^3, Z = 8, D_{calc} = 1.3 83 g cm^{-3}, μ = 0.869 mm^{-1}, 25947 reflections collected, 7970 unique (R_{int} = 0.0644), $R1$ = 0.0613, $wR2$ = 0.1607 [$I > 2\sigma(I)$].

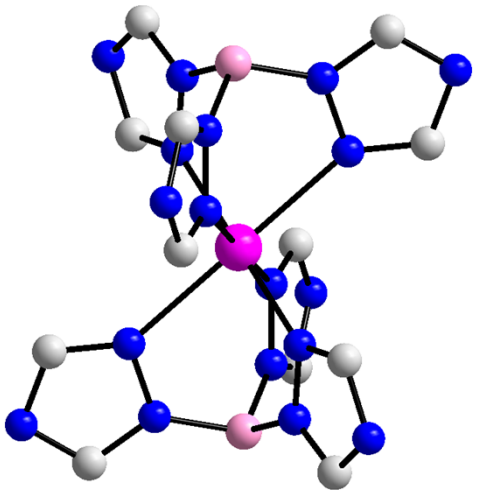

Fig. S1. Molecular structure of $[Cu(Tt)_2]$.

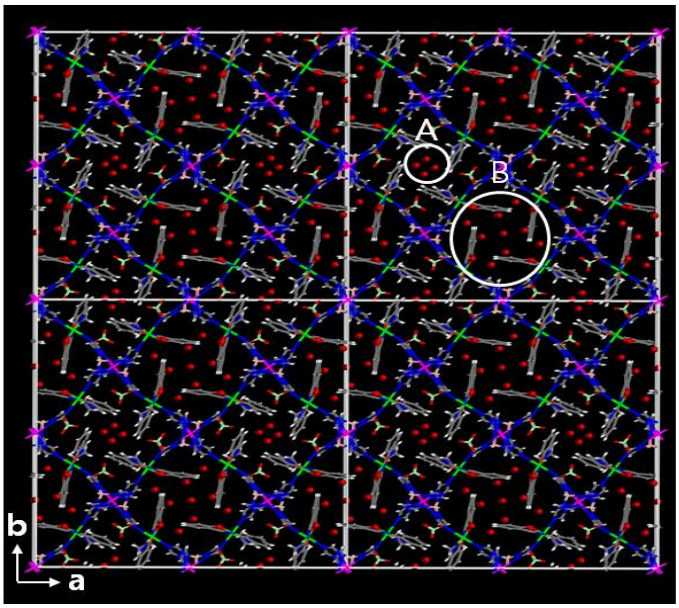

(a)

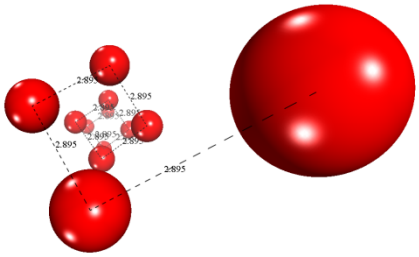

(b)

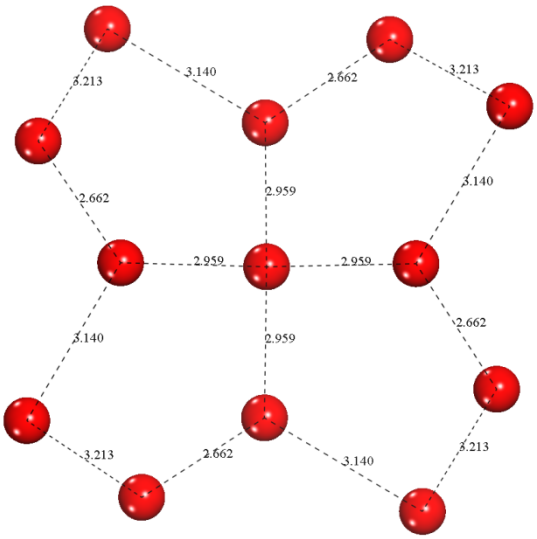

(c)

Fig. S2. (a) Extended view of **1** in the *ab* plane. Two types of hydrogen-bonded water molecules (denoted as A and B) are in the pores. (b) Perspective view of A highlighting hydrogen-bonded helical water chain s running along the *c* axis. (c) Hydrogen-bonded water clusters of B where the central atom is at the cente r of a tetrahedron with four corner atoms.

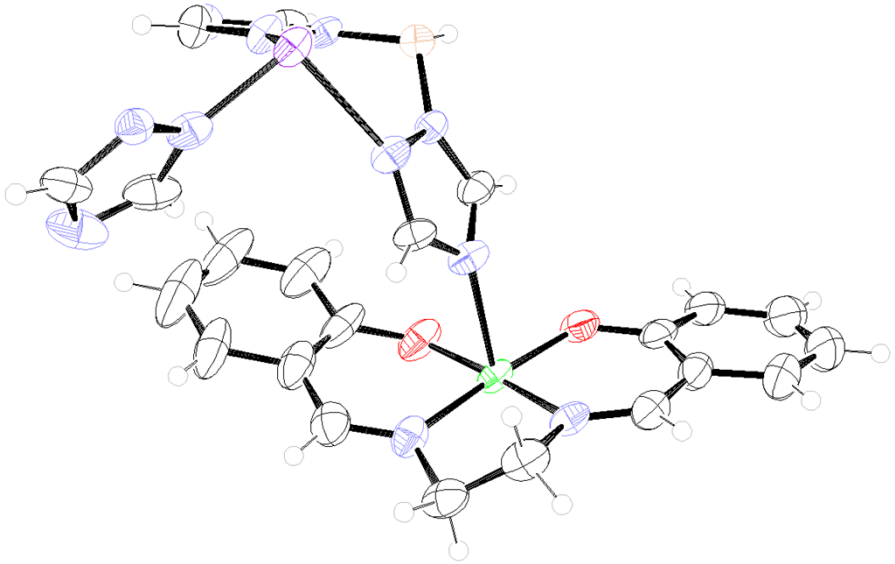

(a)

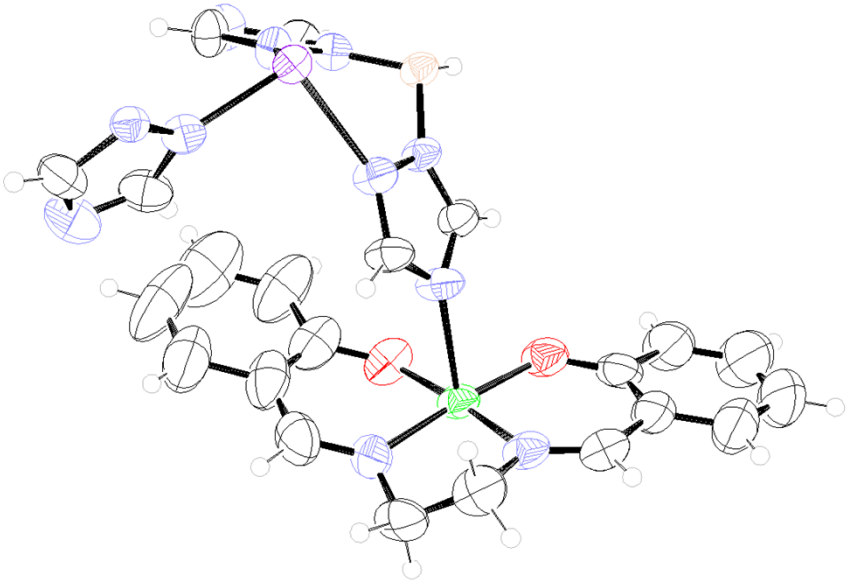

(b)

Fig. S3. ORTEP drawing of (a) **1** and (b) **1'** with thermal ellipsoids (C: black, N: blue, O: red, B: brown, Mn: green, and Cu: purple).

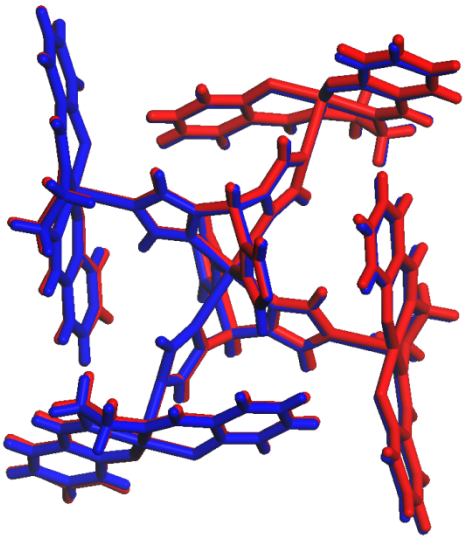

Fig. S4. Overlay structure of **1** (red) and **1'** (blue).

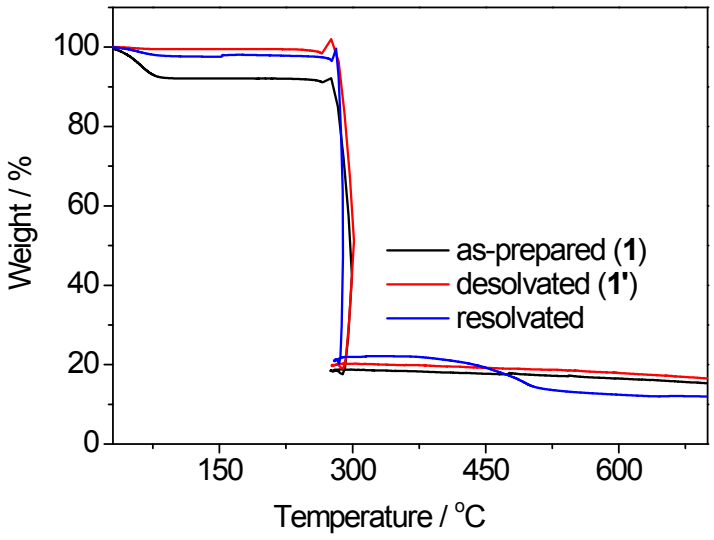

Fig. S5. TGA plots of as-prepared (**1**), dehydrated (**1'**), and resolvated samples. The anomaly at around 275 °C is due to the explosive decomposition of ClO_4^- anions. The resolvated phase has two water molecules per $CuMn_2$, which can be compared with seven water molecules per $CuMn_2$ for **1**.

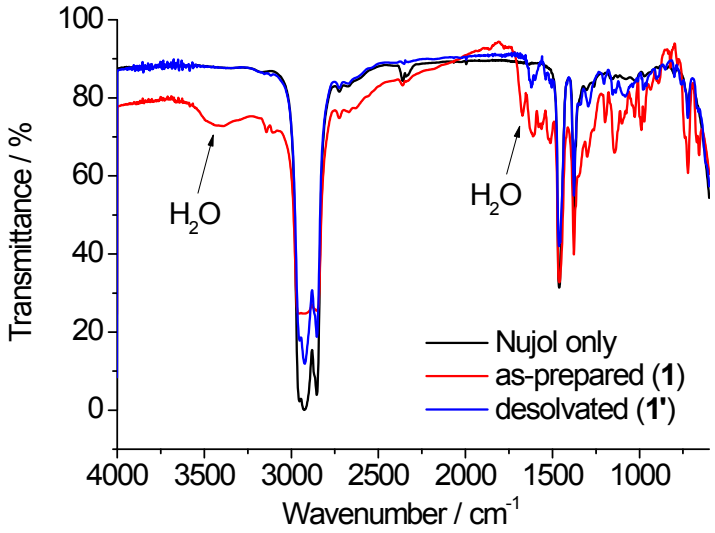

Fig. S6. Nujol IR spectra of as-prepared (**1**) and dehydrated (**1'**) samples.

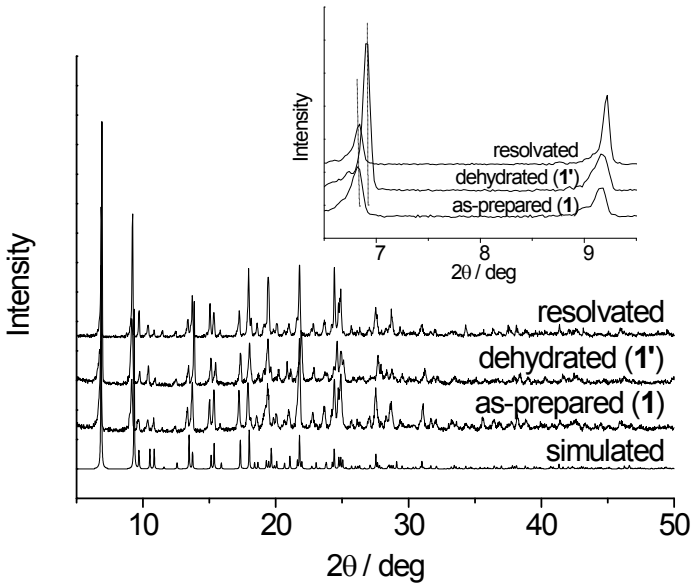

Fig. S7. PXRD patterns of the simulated (**1**), as-prepared (**1**), dehydrated (**1'**), and resolvated samples. The inset shows the enlargement of the low angle data.

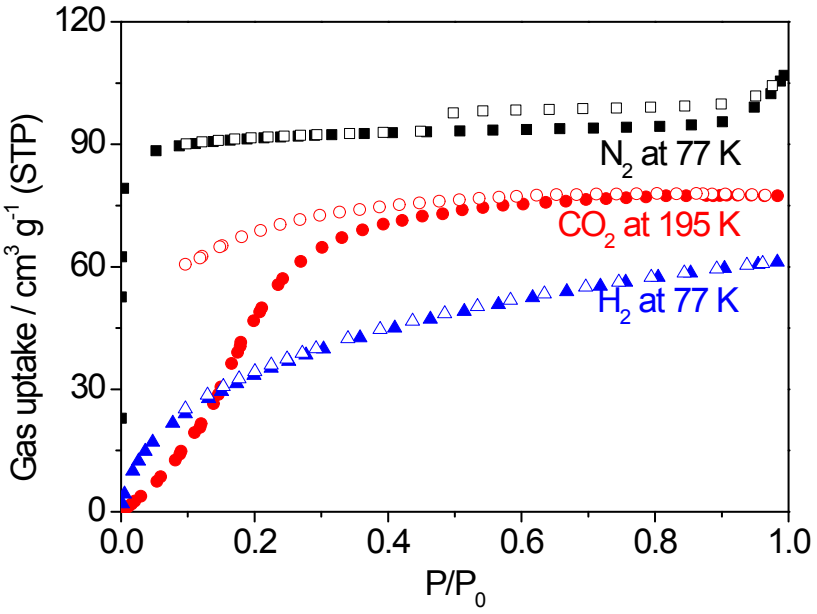

Fig. S8. Gas sorption isotherms of N_2, H_2, and CO_2 for **1'**.

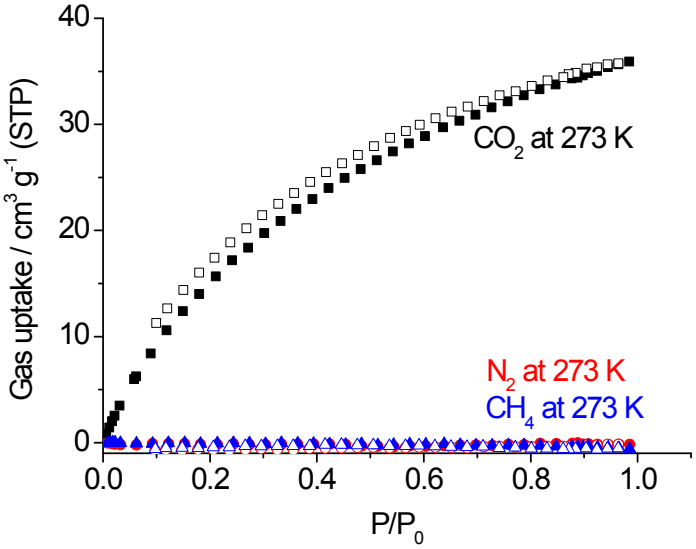

Fig. S9. Gas sorption isotherms of N_2, CH_4, and CO_2 at 273 K of **1'**.

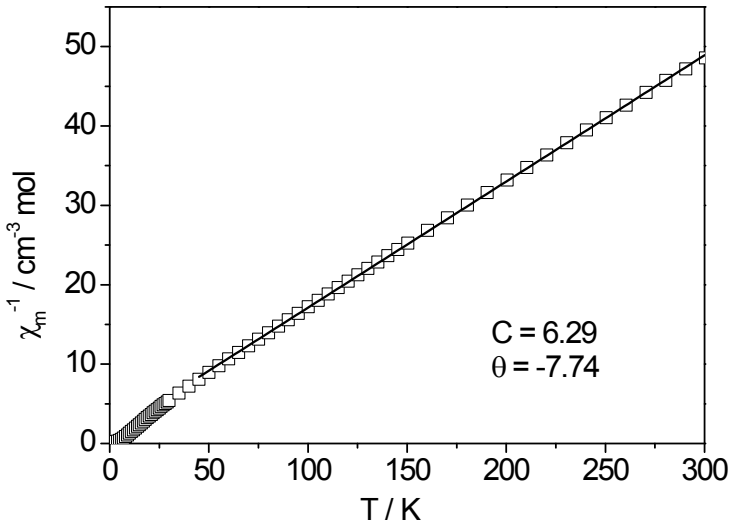

(a)

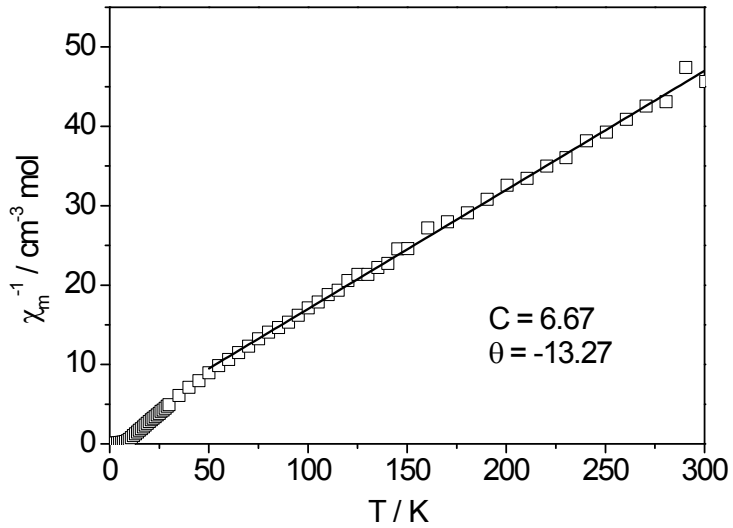

(b)

Fig. S10. Plots of χ_m^{-1} versus *T* for (a) **1** and (b) **1'** at 1000 G. The solid lines represent the best fit of the data to Cuire-Weiss law [$\chi_m = C/(T-\theta)$]. The negative values of the Weiss constants (θ) indicate the presence of antiferromagnetic couplings between neighboring spins.

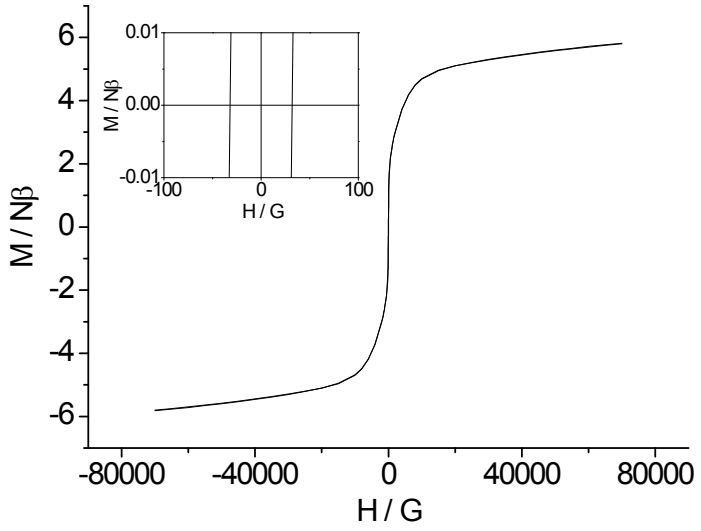

Fig. S11. Plot of *M* versus *H* of **1** at 2 K and the inset shows a blow-up at low fields.

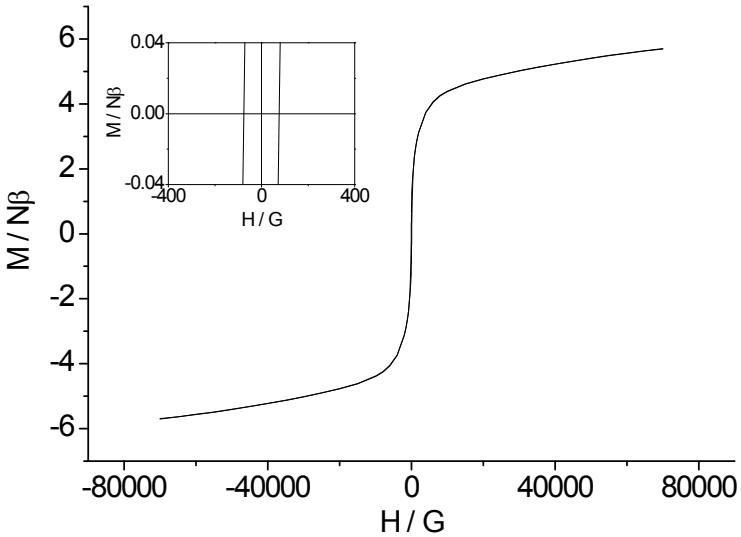

Fig. S12. Plot of *M* versus *H* of **1'** at 2 K and the inset shows a blow-up at low fields.

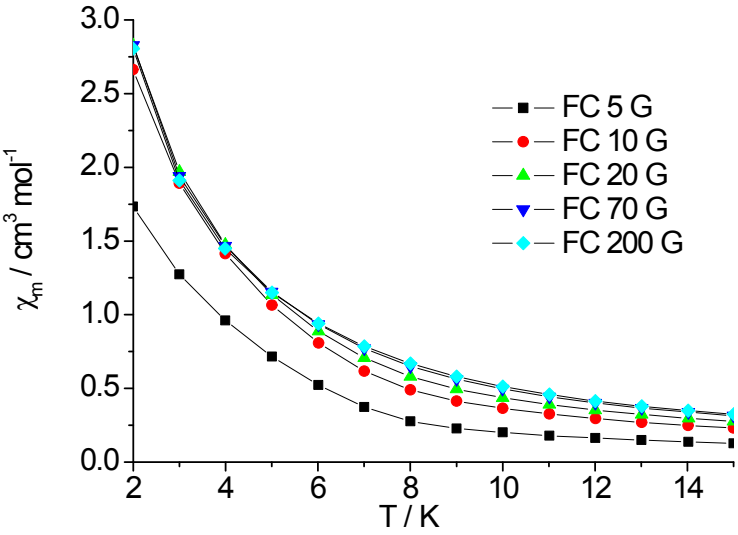

Fig. S13. Plots of field-cooled (FC) magnetic susceptibilities versus *T* of **1**.

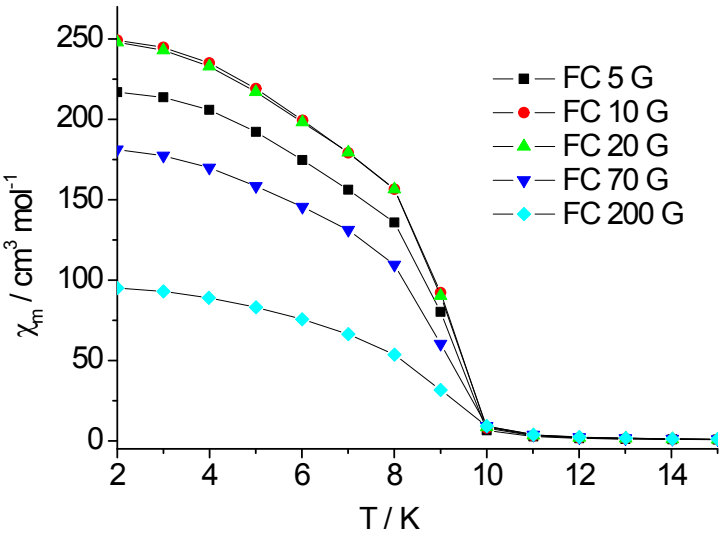

Fig. S14. Plots of FC magnetic susceptibilities versus *T* of **1**'.

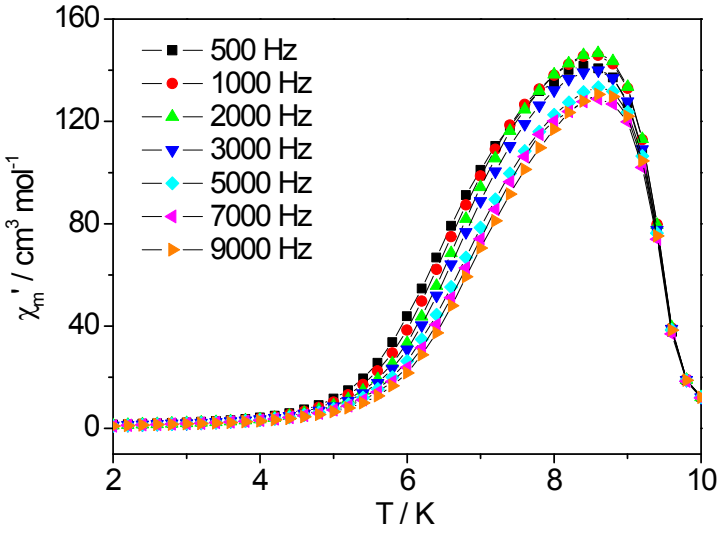

Fig. S15. Plots of χ_m' versus *T* for **1** at indicated frequencies.

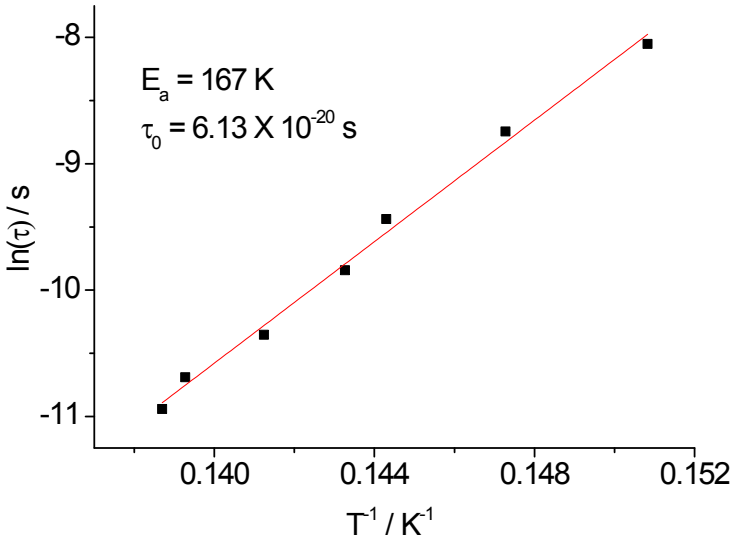

Fig. S16. Arrhenius plot for **1**.

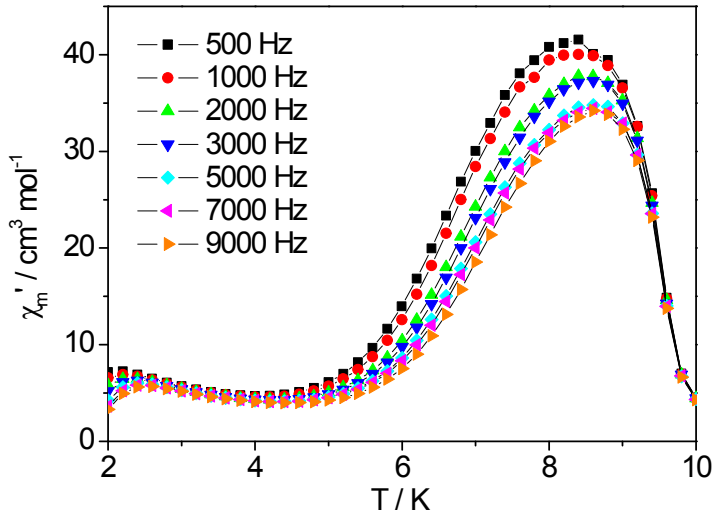

Fig. S17. Plots of χ_m' versus *T* for **1'** at indicated frequencies.

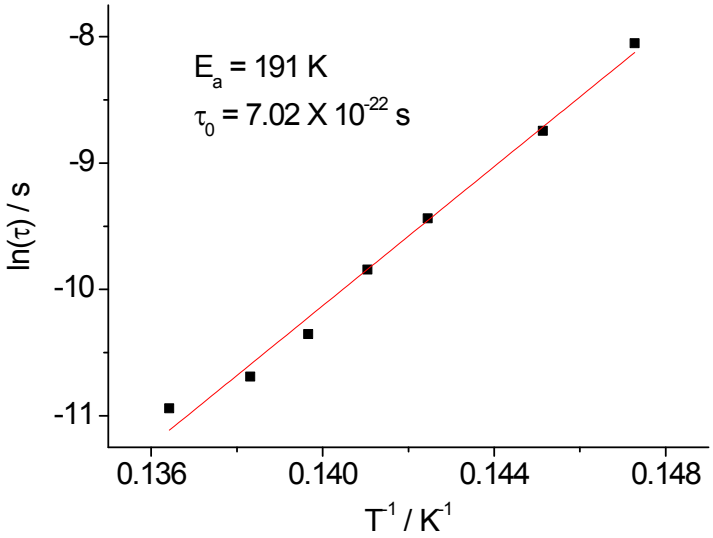

Fig. S18. Arrhenius plot for **1'** in the higher temperature region.

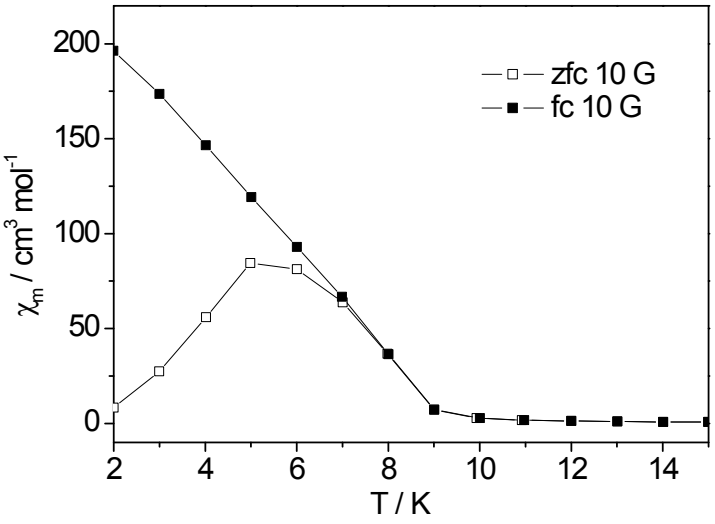

Fig. S19. Plot of ZFC/FC curves for the resolvated sample at 10 G.

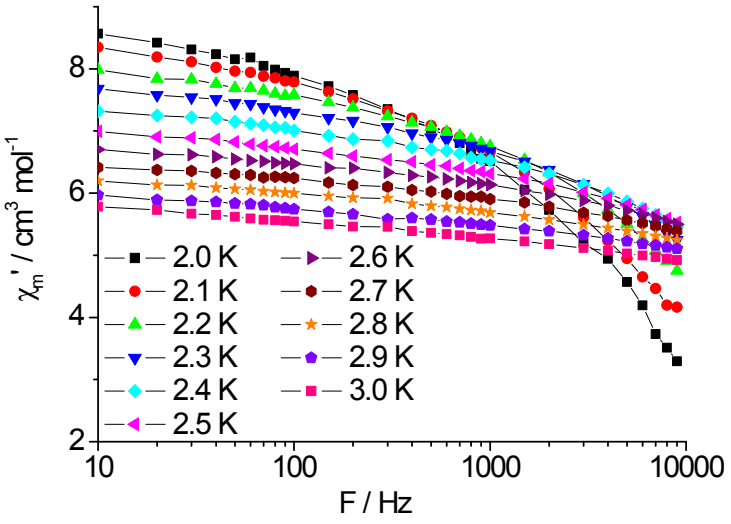

(a)

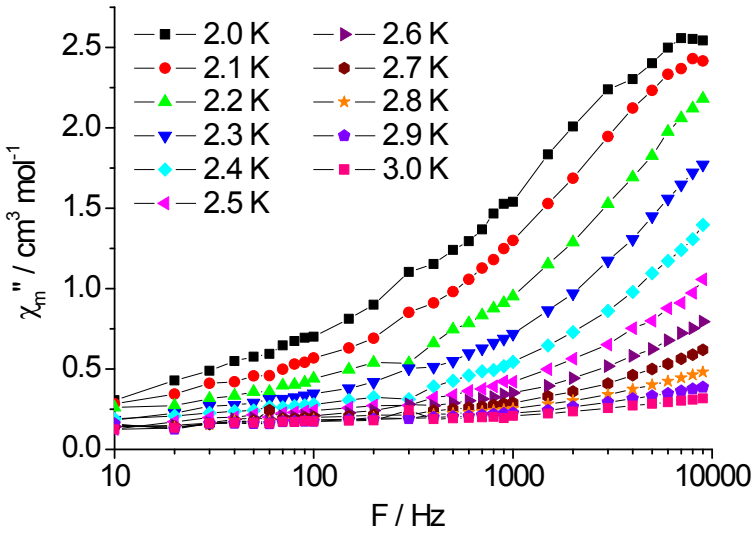

(b)

Fig. S20. Plots of (a) χ_m' and (b) χ_m'' versus *f* for **1'** at indicated temperatures.

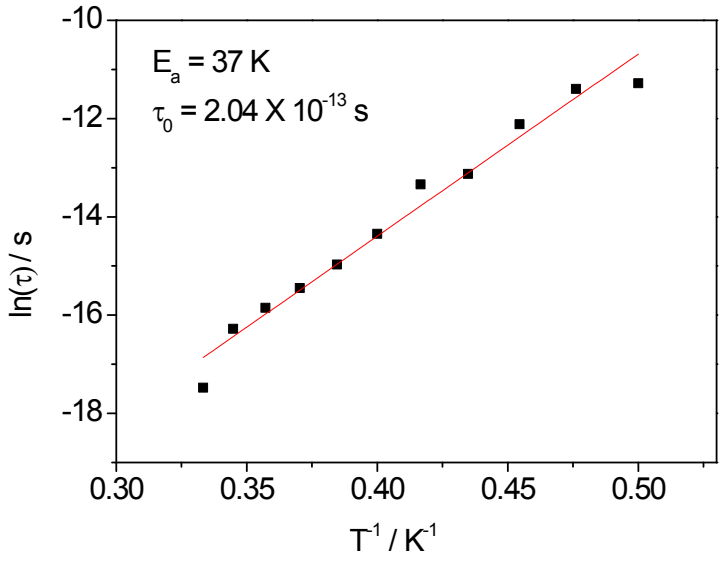

Fig. S21. Arrhenius plot for **1'** in the lower temperature region.

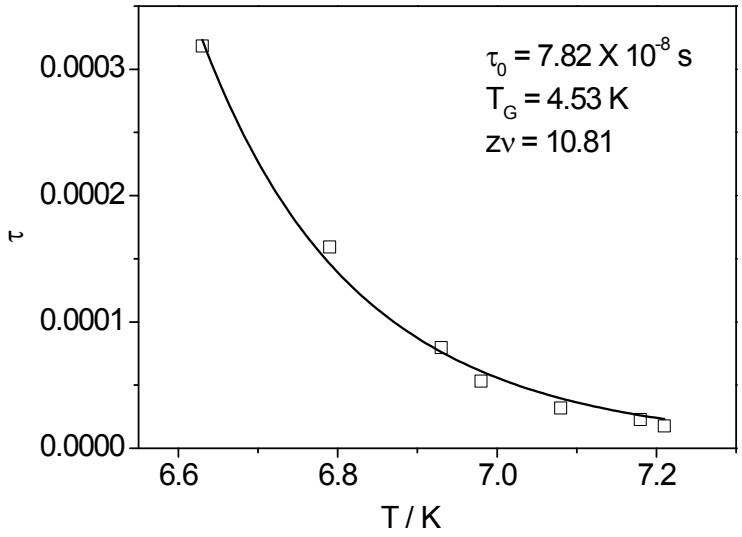

(a)

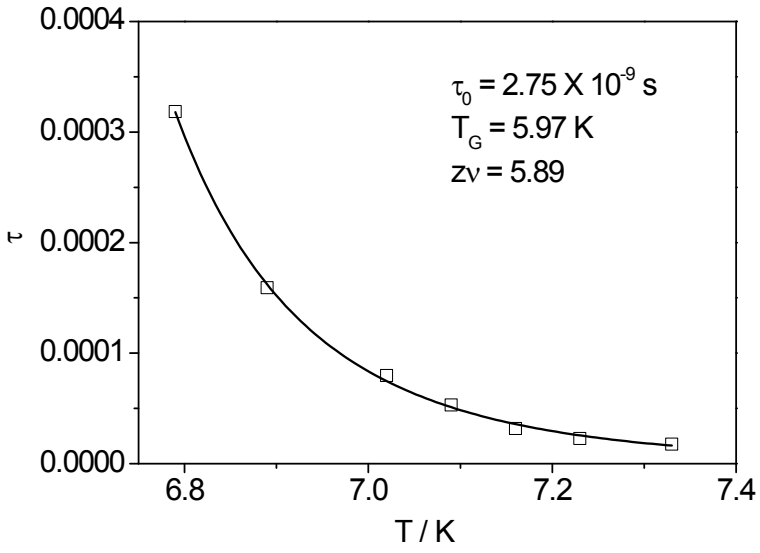

(b)

Fig. S22. Plots of τ versus temperature for (a) **1** and (b) **1'**. The solid lines represent the best fits of the dat a to the critical scaling law, $\tau/\tau_0 = (T_f/T_G - 1)^{-z\nu}$. The zν value falls in the range for spin glasses.